Laser Light Scattering Characterization of Special Intractable Macromolecules in Solution

Chi Wu

Department of Chemistry, The Chinese University of Hong Kong, Shatin, N.T. Hong Kong, China
E-mail: chiwu@cuhk.edu.hk

This review summerizes the recent advances in characterization of some special intractable macromolecules in solution by laser light scattering. Since both static and dynamic laser light scattering (LLS) are theoretically well established, we focus the discussion on experimental details, such as the design of a high-temperature LLS spectrometer, the sample clarification, a novel differential refractometer, and some newly developed methods for data analysis which include a combination of static and dynamic LLS leading to molar mass distribution determination and LLS calibration of gel permeation chromatography.

Advances in Polymer Science, Vol. 137

List of Symbols and Abbreviations

Sect. 1

LLS	laser light scattering
GPC	gel permeation chromatography
FFF	field flow fractionation
$<M>$	average molecular weight
β	an integer number
M	molecular weight for monodisperse species
M_n	number-average molecular weight
M_w	weight-average molecular weight
M_z	intensity-average (z-average) molecular weight
$f_n(M)$	differential number distribution

Sect. 2

I(t)	scattering intensity at time t
n(t)	scattering photon counts at time t
$R_{vv}(\theta)$	excess Rayleigh ratio at angle θ
$<I>_{solution}$	time-averaged scattering intensity of solution
$<I>_{solvent}$	time-averaged scattering intensity of solvent
$<I>_{standard}$	time-averaged scattering intensity of standard
$<I>$	time-averaged scattering intensity
$R_{vv,standard}(\theta)$	Rayleigh ratio of standard at angle θ
n	refractive index of solution
$n_{standard}$	refractive index of standard
a	detection geometry parameter
$<R_g^2>^{1/2}$ or $<R_g>$	root-mean square z-average radius of gyration
q	scattering vector
K	optical constant
N_A	Avogadro number
dn/dC	specific refractive index increment
λ_o	wavelength of the laser light in vacuum
C	concentration of polymer solution
A_2	second virial coefficient
QELS	quasi-elastic light scattering

$G^{(2)}(t,q)$	intensity-intensity time correlation function at q and delay time t
t	time variable
t	delay time variable
PCS	photon correlation spectroscopy
$g^{(1)}(t,q)$	normalized first-order electric field time correlation function at q and delay time t
A	baseline
β	coherence parameter
I(t,q)	scattered intensity at time t and q
CONTIN	Laplace inversion program
$G(\Gamma)$	line-width distribution
Γ	line-width for monodisperse species
E(t,q)	scattered electric field at time t and q
$<\Gamma>$	average line-width
D	translational diffusion coefficient
k_d	diffusion second virial coefficient
f	dimensionless parameter
G(D)	translational diffusion coefficient distribution
<D>	average translational diffusion distribution
G	proportionality factor

Sect. 3

PPTA or Kevlar	poly(1,4-phenyleneterephthalamide)
Teflon and Tefzel	fluorocarbon polymers
PEL-PCL	poly(ethylene terephthalate-*co*-caprolactone)
Δn	refractive index difference between solvent and solution

Sect. 4

k_D	scaling constant in $D=k_D M^{-\alpha D}$
α_D	scaling constant in $D=k_D M^{-\alpha D}$
$f_w(M)$	differential weight distribution
$M_{w,calcd}^{DLS}$	weight-average molecular weight calculated on the basis of G(D) from DLS
$M_{w,measd}$	weight-average molecular weight measured from static LLS
ERROR(α_D)	error function of α_D
ERROR(k_D)	error function of k_D
$[\eta]$	intrinsic viscosity
k_η	scaling constant in $[\eta]=k_\eta M^{-\alpha\eta}$
α_η	scaling constant in $[\eta]=k_\eta M^{-\alpha\eta}$
$F_{w,cum}(M)$	cumulative weight distribution
SEC	size-exclusion chromatography
V	elution volume
A	calibration constant in $V=A+B \log (M)$
B	calibration constant in $V=A+B \log (M)$
C(V)	elution volume distribution

$M_{w,calcd}^{SEC}$	weight-average molecular weight calculated on the basis of C(V) from GPC

Sect. 5

$M_{w,app}$	apparent weight-average molecular weight
ν	refractive index increment for the whole sample
$\nu(M)$	refractive index increment for copolymer with molecular weight M and weight distribution $f_w(M)$
$w_A(M)$	weight fraction of A for a given polymer chain with fixed M and $F_w(M)$
$w_B(M)$	weight fraction of B for a given polymer chain with fixed M and $F_w(M)$
ν_A	refractive index increment of polymer A
ν_B	refractive index increment of polymer B
w_A	weight fraction of A
w_B	weight fraction of B
ν_{s1}	ν in solvent 1
ν_{s2}	ν in solvent 2
$\nu_{A,s1}$	ν_A in solvent 1
$\nu_{B,s1}$	ν_B in solvent 1
$\nu_{A,s2}$	ν_A in solvent 2
$\nu_{B,s2}$	ν_B in solvent 2
$f_{w,app(M),s1}$	apparent weight distribution in solvent 1
$f_{w,app(M),s2}$	apparent weight distribution in solvent 2
$M_{w,L}$	low weight-average molecular weight polymer
$M_{w,H}$	high weight-average molecular weight polymer
X_L	weight fraction of low molecular weight polymer
X_H	weight fraction of high molecular weight polymer
$G_L(\Gamma)$	line-width distribution for low molecular weight polymer
$G_H(\Gamma)$	line-width distribution for high molecular weight polymer
A_L	area covered by $G_L(\Gamma)$
A_H	area covered by $G_H(\Gamma)$
A_r	area ratio A_L/A_H
R	radius of a colloidal particle
ϱ	density of particle
$(M_w)_{cal}$	calculated weight-average molecular weight
b	thickness of the hydrodynamic layer

1 Introduction

Differing from small molecules, typical polymers have an average molar mass of ~10^4 g/mol or higher and a wide distribution of chain length. For a given type of polymer, its properties, even its appearance, are greatly influenced not only by its average molecular weight, but also by its molecular weight distribution.

Therefore, the development and application of a polymer often require a precise characterization of these quantities.

A number of methods including laser light scattering (LLS) are routinely used to determine the average molecular weights and molecular weight distribution of a polymer. They include end-group chemical analysis, vapour pressure osmometry, membrane osmometry, sedimentation equilibrium, static (classic) LLS and very recently developed matrix-assisted time-fly mass spectroscopy as absolute methods in the sense that these do not require a calibration with a set of narrowly distributed polymer samples with known molecular weights. The relative methods include viscometry, gel permeation chromatography (GPC), field flow fractionation (FFF) and dynamic LLS.

The average molecular weight <M> of a polydisperse polymer sample is generally defined by

$$<M> = \int_0^\infty f_n(M)M^\beta \, dM \; / \; \int_0^\infty f_n(M)M^{\beta-1} \, dM \qquad (1.1)$$

if β is an integer, where $f_n(M)$ is the number distribution of molecular weight M. Thus, $\beta=1$ for the number-average molecular weight (M_n), $\beta=2$ for the weight-average molecular weight (M_w) and $\beta=3$ for z-average molecular weight (M_z). For example, M_n is measured by end-group analysis and osmometry; M_w, by GPC, sedimentation equilibrium and static LLS; and M_z, by sedimentation equilibrium and dynamic LLS. In practice, the ratio of M_w/M_n is called the polydispersity index and is conveniently used to characterize the distribution width of a given polymer sample.

Static light scattering as a classic and absolute method has been long and widely used to characterize both synthetic and natural macromolecules [1–4]. In the last two decades, thanks to the advances in stable laser, ultra-fast electronics and personal computers, laser light scattering (LLS), especially dynamic LLS (denoted here by DLS), has gradually changed from a very special tool for physical chemists to a routine analytical tool in polymer laboratories or even to a daily quality-control device in production lines [5–8]. The LLS instruments commercially available nowadays are normally capable of making both static and dynamic measurements simultaneously.

2
Basic Principles of Laser Light Scattering

When a monochromatic, coherent light is incident into a dilute macromolecule solution, if solvent molecules and macromolecules have different refractive index, the incident light is scattered by each illuminated macromolecule to all directions [9, 10]. The scattered light waves from different macromolecules mutually interfere, or combine, at a distant, fast photomultiplier tube detector and produce a net scattering intensity I(t) or photon counts n(t) which is not uniform on the detection plane. If all macromolecules are stationary, the scattered light intensity at each direction would be a constant, i.e. independent of time.

However, in reality, all macromolecules in solution are undergoing constant Brownian motion, and this fact leads to fluctuation in I(t). The fluctuation rate can be related to the translational diffusion of the macromolecules. The faster the diffusion, the faster the fluctuation will be.

2.1 Static Laser Light Scattering

In static LLS, the angular dependence of the excess absolute time-averaged scattered intensity, known as the excess Rayleigh ratio, $R_{vv}(\theta)$, is normally measured, where $R_{vv}(\theta)=(<I>_{solution}-<I>_{solvent})/<I>_{standard} \cdot R_{vv,standard}(\theta) \cdot (n/n_{standard})^a$ with <I> and n denoting the time-averaged scattering intensity and the refractive index, respectively, and $1 \le a \le 2$ depending on the detection geometry. Thus, if the scattering volume is selected by a slit, a=1, and if the scattering volume is selected by a pinhole much smaller than the beam diameter, a=2. If the solution is very dilute, $R_{vv}(\theta)$ at a relatively small scattering angle θ can be related to the weight-average molecular weight M_w, the second virial coefficient A_2 and the root-mean square z-average radius of gyration $<R_g^2>^{1/2}$ (or written as $<R_g>$ for simplicity) by the expression [9, 10]

$$\frac{KC}{R_{(vv)}(\theta)} \approx \frac{1}{M_w}\left(1 + \frac{1}{3}<R_g^2>q^2\right) + 2A_2C + \ldots \qquad (2.1)$$

where C is the mass concentration of the polymer component, $K=4\pi^2n^2(dn/dC)^2/(N_A\lambda_o^4)$ and $q=(4\pi n/\lambda_o)\sin(\theta/2)$, with N_A, dn/dC, n and λ_o being the Avogadro constant, the specific refractive index increment, the solvent refractive index, and the wavelength of the laser light in vacuum, respectively. With $R_{vv}(\theta)$ measured at a series of C and θ, we can determine M_w, R_g, and A_2 by use of a Zimm plot, which allows both θ and C extrapolations to be made on a single grid [11]. Figure 1 shows a Zimm plot for an alternating copolymer of ethylene and tetraflu-

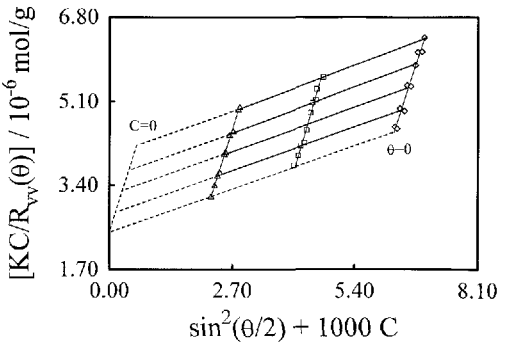

Fig. 1. Typical Zimm plot for an alternating copolymer of ethylene and tetrafluoroethylene ($M_w = 5.4 \times 10^5$ g/mol, $R_g = 45.4$ nm and $A_2 = 1.97 \times 10^{-4}$ mol mL/g^2) in diisobutyl adipate at 240 °C

oroethylene (M_w=5.4×10^5 g/mol, R_g=45.4 nm and A_2=1.97×10^{-4} mol mL/g^2) in diisobutyl adipate at 240 °C [12]. It should be noted that Eq. (2.1) is valid under the restriction that the polymer solution exhibits no adsorption, no fluorescence, and no depolarized scattering. As for rigid and nearly rigid rods causing depolarized scattering, readers can refer to the excellent review article of Russo and the references therein [13]. As for the correction of adsorption and fluorescence, readers are advised to refer to the characterization of Kevel in concentrated sulfuric acid by Qing *et al.* [14–16].

2.2 Dynamic Laser Light Scattering

DLS measures the intensity fluctuation instead of the average light intensity (this is where the word 'dynamic' comes from), and its essence may be explained as follows. When the incident light is scattered by a moving macromolecule or particle, the detected frequency of the scattered light will be slightly higher or lower than that of the original incident light owing to the Doppler effect, depending on whether the scatterer moves towards or away from the detector. Thus, the frequency distribution of the scattered light is slightly broader than that of the incident light. This explains why dynamic light scattering is sometimes called quasi-elastic light scattering (QELS). The frequency broadening (~10^5–10^7 Hz) is so small in comparison with the incident light frequency (~10^{15} Hz) that, if not impossible, it is very difficult to detect it. However, it can be effectively recorded in the time domain through an intensity-intensity time correlation function $G^{(2)}(t,q)$ in the self-beating mode. Thus, dynamic light scattering is also known as photon correlation spectroscopy (PCS).

$G^{(2)}(t,q)$ can be related to the normalized first-order electric field time correlation function $|g^{(1)}(t,q)|$ by [9, 10]

$$G^{(2)}(t,q) = \langle I(t,q)I(0,q)\rangle = A[1+\beta|g^{(1)}(t,q)|^2] \tag{2.2}$$

where A is the measured base line, β is a parameter depending on the coherence of the detection optics, and t is the delay time.

For a monodisperse sample, $g^{(1)}(t,q)$ is theoretically represented by

$$g^{(1)}(t,q) = Ge^{-\Gamma t} \tag{2.3}$$

where G and Γ are the proportionality factor and the line-width respectively. For dilute solutions, Γ measured at a finite scattering angle is related to C and q by [17]

$$\Gamma = q^2 D(1+k_d C)(1+f\langle R_g^2\rangle_z q^2) \tag{2.4}$$

Here D is the translational diffusion coefficient of the solute molecule at $C \rightarrow 0$ with C the mass concentration of the solute, k_d the diffusion second virial coefficient, f a dimensionless parameter depending on polymer chain structure and solvent, and $<R_g^2>$ the mean square radius of gyration of the polymer chain. Hence, for C and q small enough, Eq. (2.3) may be approximated by

$$g^{(1)}(t,q) = Ge^{-q^2Dt} \tag{2.5}$$

The proportionality factor G may depend on many characteristics of the solute polymer, but since D is the only polymer-dependent variable in Eq. (2.5), it is reasonable here to treat G as a function of D only for a homologues series of polymers. Thus, for a polydisperse polymer sample with a continuous distribution of molecular weight M, Eq. (2.5) may be generalized as

$$g^{(1)}(t,q) = \int_0^\infty G(D)e^{-q^2Dt}dD \tag{2.6}$$

where G(D) is called the translational diffusion coefficient distribution. This equation is the basic of the entire discussion in the present paper. Note that since $g^{(1)}(t,q) \rightarrow$ unity as t goes to zero, we have

$$\int_0^\infty G(D)dD = 1 \tag{2.7}$$

that is, G(D) is normalized. Equation (2.6) indicates that once $g^{(1)}(t,q)$ is determined from $G^{(2)}(t,q)$ through Eq. (2.2), G(D) can be computed by Laplace inversion [18–24]. Among many others, the program called CONTIN [24] is one of the most widely used and accepted for this computation. However, due to the bandwidth limitation of photon correlation instruments, some unavoidable noises, and a limited number of data points, the data obtained for $g^{(1)}(t,q)$ do not always provide information necessary and sufficient to determine $G(\Gamma)$ uniquely. This difficulty is well-known as the ill-posed problem. Thus, in practice, reducing the noises in the measured $G^{(2)}(t,q)$ becomes more important than choosing a program for data analysis.

Figure 2 illustrates the $g^{(1)}(t,q)$ data for chitosan ($M_w=1.06\times10^5$ g/mol and $<D>=5.92\times10^{-8}$ cm^2/s) in aqueous 0.2 *M* CH_3COOH/0.1 *M* CH_3COONa at 25 °C, $\theta=45°$ and $C=4.96\times10^{-4}$ g/ml. Here, <D> is the average diffusion coefficient given by

$$<D> = \int_0^\infty G(D)DdD \tag{2.8}$$

Figure 3 shows the G(D) function for the same system as in Fig. 2 at $\theta \rightarrow 0$ and $C \rightarrow 0$.

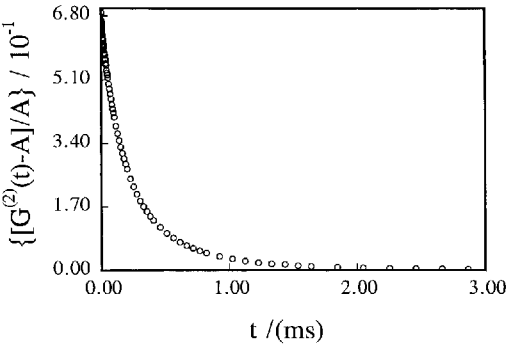

Fig. 2. Typical normalized intensity-intensity time correlation function for chitosan ($M_w = 1.06 \times 10^5$ g/mol and $\langle\Gamma\rangle = 2.19$ ms) in 0.2 *M* CH_3COOH / 0.1 *M* CH_3COONa aqueous solution at T = 25 °C, $\theta = 45°$ and $C = 4.96 \times 10^{-4}$ g/mol

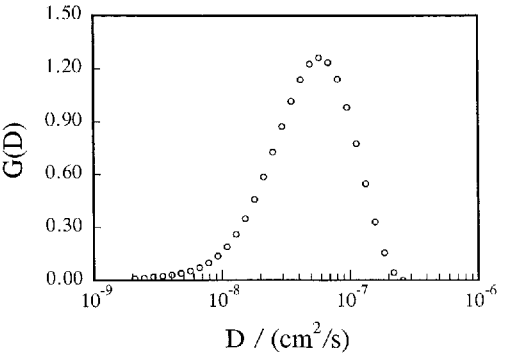

Fig. 3. Typical translational diffusion coefficient G(D) for chitosan ($M_w = 1.06 \times 10^5$ g/mol and $\langle D\rangle = 5.92 \times 10^{-8}$ cm^2/s) in 0.2 *M* CH_3COOH / 0.1 *M* CH_3COONa aqueous solution at T = 25 °C, $\theta \rightarrow 0$ and $C \rightarrow 0$

3 Experimental Section

3.1 Solvent Selection

If a macromolecule can be dissolved in more than one solvent, the choice of the solvent for laser light scattering measurement should be made generally according to the following three criteria: 1) it is colorless so that the adsorption correction can be avoided, 2) it has a higher contrast, i.e. a higher value of the spe-

cific refractive index increment dn/dC, so that the signal-to-noise ratio is increased, and 3) it is less polar and less viscous so that the solution may be clarified more easily.

Sometimes in practice, we may have no choice of solvent for a given polymer. For example, poly(1,4-phenyleneterephthalamide) (PPTA or Kevlar) is only soluble in very strong acids which are viscous. In such cases, ultracentrifugation instead of filtration has to be used to remove dust particles from the solution [14–16, 25]. As for copolymers, the selection of proper solvents is even more difficult, because at least two solvents which satisfy the above mentioned three criteria are needed. For this reason, reported characterization of copolymers is quite limited [26–29].

One of the challenging problems in the application of LLS methodology is to study static and dynamic properties of fluorocarbon polymers, such as Teflon and Tefzel (registered trademarks of Du Pont), which defy the characterization owing to their insolubility in ordinary solvents. It is this unique solubility that makes these fluorocarbon polymers very useful in many applications, but greatly annoys those who wish to explore their solution properties. However, it was found that some solvents were capable of dissolving them at high temperature, but the finding was not enough to solve all characterization problems because the technique for clarification and measurement of the solutions at high temperature remained to be established.

3.2 High-Temperature Spectrometer

In order to characterize a polymer soluble only at high temperature, many difficulties had to be overcome before light-scattering measurement was actually made. Thus, a special high-temperature LLS spectrometer was first designed and developed at State University of New York in Stony Brook, and then its technique was transferred to both Du Pont and BASF [30–35].

Figure 4 shows a schematic diagram of the high-temperature LLS spectrometer at Du Pont. In it, a thermally-controllable plate (13) used as a heat sink isolates the rotary table (12) from the outer thermostat (3) by means of two sets of stainless steel standoffs (14). The outer brass thermostat (3) is isolated from the room with 0.5-in.-thick porous silicone rubber. This arrangement creates an oven that allows the temperature to keep easily in the 320–340 °C range with temperature fluctuations of less than 0.2 °C. A glass (vacuum) jacket of 2.25-in. o.d. isolates the inner thermostat from the oven. The vacuum jacket reduces the temperature gradient in the light scattering cell. The inner thermostat has a separate temperature controller and a miniature platinum resistance thermometer that can be connected to a digital voltmeter through the vacuum jacket by means of ceramic feed throughs. With this design, short-term (20 min) control of ±0.05 °C, intermediate-term (60 min) control of ±0.1 °C, and long-term control of ±0.5 °C can be achieved at 340 °C even in the absence of a vacuum. Long-term temperature stability depends partially on room-temperature fluctuations even in the presence of the outer thermostat and the isolation

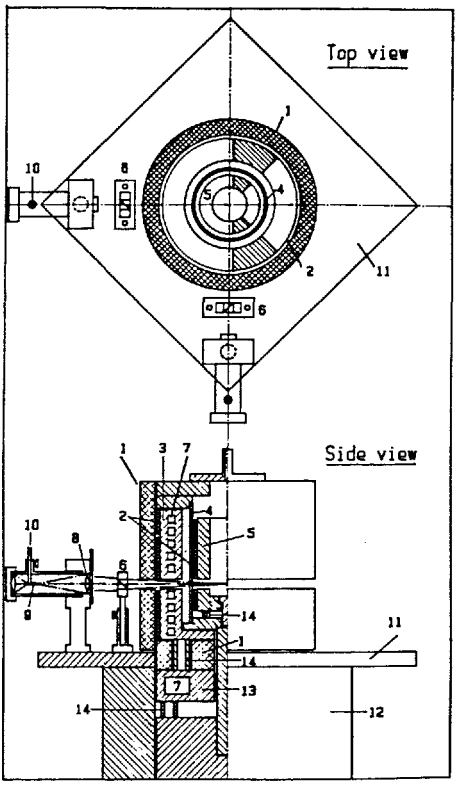

Fig. 4. Schematic top and side views of the high-temperature thermostat and detection system of the light scattering spectrometer: (1) silicon rubber insulation; (2) heating wires for the brass thermostats; (3) outer brass thermostat with fluid circulation facilities; (4) vacuum glass jacket for thermal isolation made of precision polished glass of 2.25-in. o.d. with Kovar seals at both ends of a stainless-steel temperature shield with precision polished glass of 2.25-in. o.d.; (5) inner brass thermostat, which has a separate temperature controller and a thermometer and can accommodate a light scattering cell up to 27-mm o.d; (6) Glan-thompson polarizers; (7) fluid circulation paths; (8) lens; (9) field aperture; (10) optical fiber bundle; (11) rotating plate for multiple detectors; (12) RT-200 Klinger rotary table with 0.01° step size; (13) cooling plate to isolate the outer thermostat from the rotary table; and (14) stainless steel standoffs for thermal isolation

between the two thermostats. Figure 5 shows typical temperature fluctuations of the inner thermostat at 340 °C. To mention more, a high-temperature LLS detector coupled with GPC has recently been developed and the determination of the molar mass distribution of poly(phenylene sulfide) in 1-chloronaphthalene at 220 °C has been made possible with it [36]. The advantage of on-line coupling LLS with GPC is obvious, since GPC is a fractionation method and LLS allows an absolute molar mass measurement and hence makes the calibration of GPC columns.

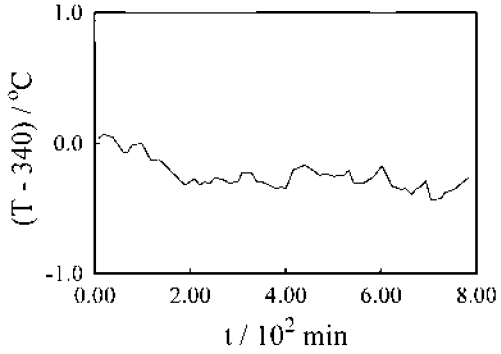

Fig. 5. Typical temperature fluctuations in the inner thermostat at 340 °C. Intermediate-term (1 h) temperature fluctuations were ± 0.1 °C. Long-term (10 h) temperature fluctuations were ± 0.5 °C

3.3 Solution Preparation at High Temperature

In order to prepare and clarify a polymer solution at a temperature higher than 200 °C, two different apparatuses were developed [30, 33]. Importantly, they are able (1) to dissolve a polymer under an inert atmosphere without losing solvent and without building up inner pressure due to solvent evaporation, and (2) to transfer the solution into a filtration device by a remote control.

Figure 6 shows a specially designed dissolution/filtration apparatus which can be placed inside a small oven. Known weights of a polymer sample and a filtered solvent, as well as a small glass-enclosed magnetic stirrer, are placed in A at room temperature. The solution vessel (A) is then connected to the precleaned filter (B). After degassing followed by introduction of nitrogen, both stopcocks are closed and the oven is heated to the desired temperature to dissolve the polymer while the solution is stirred. When the polymer is considered to have been completely dissolved, the solution vessel is turned 180° by means of the seal glass joint (J). This allows the polymer solution to be transferred from A into B without exposure to air. A gentle pressure using nitrogen is applied to force the polymer solution to pass through the fine-grade sintered glass filter (f) and to move directly into the precleaned dust-free cylindrical light scattering cell (C). In this way, dust-free polymer solutions can be successfully prepared, keeping the temperature high.

Figure 7 shows another type of dissolution/filtration apparatus. Sleeve A (with no bottom) is joined to the shaded stopper, which is connected to a reflux condenser by means of a greaseless glass joint. Cup (B), with a magnetic stirrer (E) sitting on top of the fine-grade sintered glass filter (F_2), allows solution clarification. First, a dust-free solvent and a polymer are placed in B of the argon-filled apparatus which has the preattached dust-free light-scattering cell (D). The reflux condenser flushed with argon is then inserted taking care that the apparatus with the polymer and solvent is under an inert atmosphere at room tem-

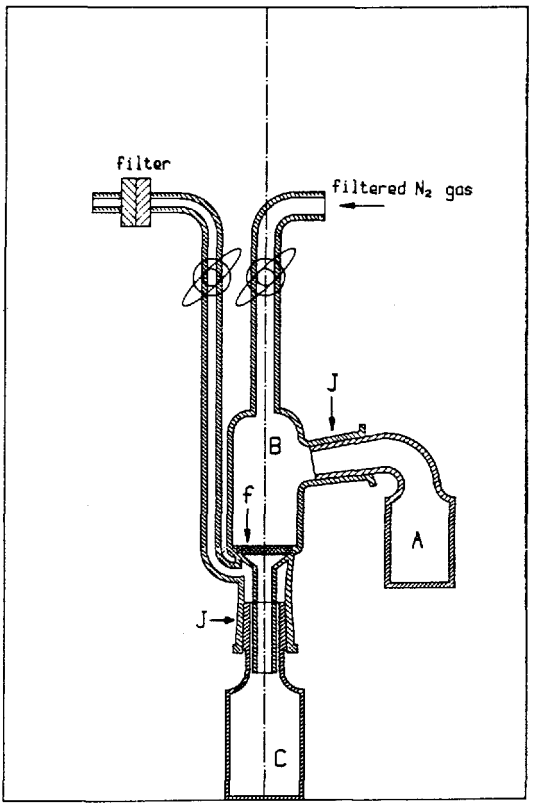

Fig. 6. High-temperature dissolution/filtration apparatus. The entire apparatus is placed in a high-temperature oven controlled at 250 ± 2 °C. (A) Solution vessel, where known weights of polymer and solvent as well as a small glass-enclosed magnetic stirrer are introduced. (B) a fine-grade sintered glass filter, connected to A and C by means of clean seal glass joints (J) (14/20, Wheaton Scientific). (f) Fine-grade sintered glass filter. (C) Cylindrical light scattering cell of 27-mm o.d. with a clean seal glass joint

perature. The entire apparatus is set in a small oven and the temperature is raised to the desired value. When the polymer is completely dissolved, an argon pressure is applied through the sintered glass filter (F_1) to let the polymer solution move from B to C. The additional pressure difference plus gravity will filter the polymer solution directly into the dust-free light-scattering cell (D). After the filtration process is completed, the additional argon pressure is released. The stopcock above the upper filter is closed during a light-scattering experiment. Briefly, extreme care must be taken when the test solution is prepared and subjected to light scattering measurements at temperatures near the boiling point of the solvent because the pressure build-up could cause an explosion. This points to the absolute necessity of having a pressure releasing mechanism.

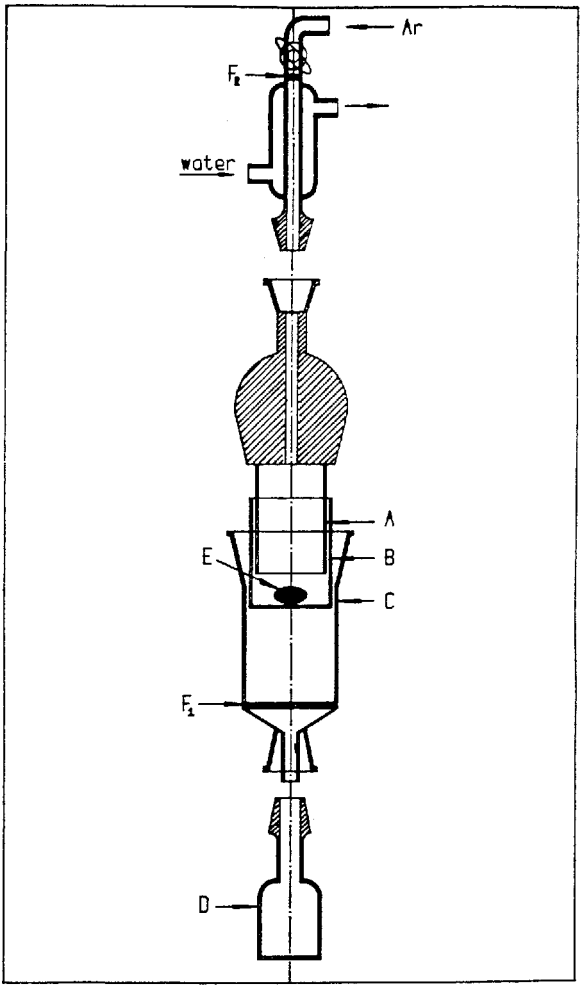

Fig. 7. Separate components of a high-temperature dissolution/filtration apparatus. The assembled apparatus, as shown in Fig. 1 of Ref. 30, is placed in a high-temperature oven. (A) Cylindrical insert (with on bottom) with a diameter ~2 mm less than that of the solution vessel (B); (C) Filtration section with a fine-grade sintered glass filter (F_1) and ground glass joints to a light scattering cell (D) and a ground glass joint adapter for the water cooled condenser which is located outside the temperature-controlled oven. (E) Magnetic stirring bar. The shaded area denotes volume reduction so that the volume accessible by vapour phase is no more than a few times the fluid phase. The miniature water-cooled condenser has a coarse-grade sintered-glass filter (F_2) so that the entire system is always isolated from external dust. The greaseless stopcock above F_2 is for operating the apparatus as a closed system, for introduction of low vacuum in order to degas the solvent before dissolution, for filling the apparatus with inert gas, such as argon, in order to alleviate chemical decomposition, and for releasing a possible pressure build-up at high temperature if chemical decomposition takes place. The entire apparatus is portable and can be inserted into the high-temperature light-scattering spectrometer with the light-scattering cell (D) and part of the filtration component (C) controlled at a given high temperature

3.4 Differential Refractometer

One of the most important parameters in static LLS is the specific refractive index increment (dn/dC), defined as $lim_{C\to o}(\partial n/\partial C)_{T,P,\lambda}$. Since this parameter is not an intrinsic property of the polymer, the conditions of fixing temperature T, pressure P and wavelength of light in vacuum λ are needed in its definition. Note that, according to Eq. (2.1), an error of E% in dn/dC will lead to an error of 2E% in the derived M_W.

The refractive index increment Dn is normally measured by using either a differential refractometer or an interferometer. In the former, light is refracted at the boundary between the sample and a reference liquid. Commonly, the beam displacement is measured directly and then converted to Δn by multiplying by a calibrated constant which can be obtained by using a solution with an accurately known refractive index difference Δn [37]. This is not an absolute method since the constant has to be calibrated under the same conditions as in the light scattering measurements. In the latter, two light beams with identical geometrical paths traverse two different optical paths. One passes through the sample and the other through the reference liquid. This method relies on the interference of the two beams. Its details can be found elsewhere [38, 39]. In a high-temperature LLS measurement, a deformed cylindrical light scattering cell is preferred to the conventional divided differential refractometer cuvette in which the exit laser beam is refracted by the solution/air interface [30].

Figure 8a shows the design of a recently developed and commercially available refractometer (ALV GmbH, Langen, Germany). A small pinhole (P) with a diameter of 400 μm is illuminated with a laser light. The illuminated pinhole is imaged to a position-sensitive detector (PD) (Hamamatsu S 3932) by a lens (L) located at an equal distance from the pinhole and the detector, where the distance is four times the focal-length (f=100 mm) of the lens. Thus, this novel refractometer uses a (2f-2f) design instead of a conventional (1f) design which uses parallel incident light beams and makes the distance between the detector and the lens equal to only one focal length. A temperature-controlled refractometer cuvette (C) (Hellma 590.049-QS) is placed just in front of the lens. It is a flow cell and has a volume of ~20 mL, which is divided by a glass plate at ~45° into two compartments. The pinhole, the cuvette, the lens and the detector are rigidly mounted on a small optical rail. The refractometer has dimensions of only 40 cm in length, 15 cm in width and 10 cm in height, and the length can be easily reduced to 20 cm with another lens if necessary. The output voltage (–10 to 10 volts) from the position-sensitive detector is proportional to the displacement of the light spot from the center of the detector, and can be measured by a digital voltmeter or an analog-to-digital data acquisition system and a personal computer.

Figure 8b shows the basic principle and the light path of the refractometer, where θ', θ'', θ''', and the cuvette are drawn enlarged to make the details clear. If both the compartments are filled with a solvent (i.e. $n=n_o$), the illuminated pinhole will be imaged at point O. However, if the solvent in one of the compartments is replaced by a dilute polymer solution with a slightly different refractive index (i.e. $n=n_o+\Delta n$), the light will be bent first by the glass plate, then by the

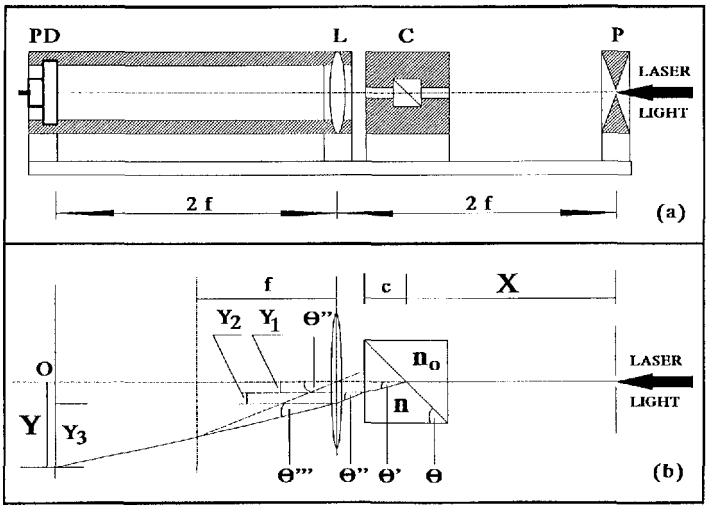

Fig. 8 a. Schematic view of a novel differential refractometer (produced by ALV GmbH, Langen, Germany), which consists of a pinhole (P), a differential refractometer cuvette (C), a lens (L, f = 10 cm) and a position sensitive detector (PD). All components are rigidly mounted on a 40 cm long optical rail. **b** Light path in which one compartment of the cuvette contains a solvent with refractive index n and the other contains a solution with slightly different refractive index $n = n_0 + \Delta n$. The cuvette and angles θ', θ'' and θ''' (actually very small, ~ 0.01 radian) are enlarged to make the light path distinct

cuvette wall and finally by the lens. The image is shifted away from the point o by a distance of Y. Figure 7b shows that

$$Y=Y_1+Y_2+Y_3=c\tan(\theta')+(2f-X-c)\tan(\theta'')+2f\tan(\theta''') \quad (3.1)$$

and

$$f\tan(\theta'')=f\tan(\theta''')+c\tan(\theta')+(2f-X-c)\tan(\theta'') \quad (3.2)$$

where c, X and θ are constants. Snell's law gives

$$n_0\sin(90-\theta)=(n_0+\Delta n)\sin(90-\theta-\theta') \quad (3.3)$$

and

$$(n_0+\Delta n)\sin(\theta')=\sin(\theta'') \quad (3.4)$$

where θ', θ'' and θ''' are actually so small because Δn is in the order of 10^{-4} RI units that we may set $\sin(\theta')=\theta'$, $\sin(\theta'')=\theta''$, $\tan(\theta')=\theta'$, $\tan(\theta'')=\theta''$ and $\tan(\theta''')=\theta'''$. Combination of Eqs (3.1)–(3.4) leads to

$$Y=K\Delta n \quad (3.5)$$

where $K=[X+c''(1-1/n_0)]\tan(90°-\theta)$. For a given optical set-up and solvent, X, c, θ, n_0, and hence K are constants. Equation (3.5) shows that the signal is proportional to Δn, and the larger the value of X, the higher the sensitivity (Y/Δn) is.

This means that the cuvette should be placed as close as possible to the lens in the experimental set-up.

In the (2f-2f) design, the detector and the pinhole (acting as a light source) are placed at the exact imagining positions along the optical axis of the lens. This configuration is optically equivalent to placing the detector directly behind the pinhole, so that the laser beam drift is eliminated. In comparison with the conventional differential refractometer, this novel design has made the measurement of Δn much easier and provides reliable and accurate values for dn/dC since it is stable and all the results can be recorded and averaged on a computer. Figure 9 shows the concentration dependence of Δn for a 13% PET-PCL copolymer in three different solvents. The lines represent the least-square fits to the data points.

The refractometer with its present dimensions can be easily installed into any existing laser light-scattering spectrometer together with the laser source, the thermostat and the computer, as exemplified in Fig. 10. The optical glass plate

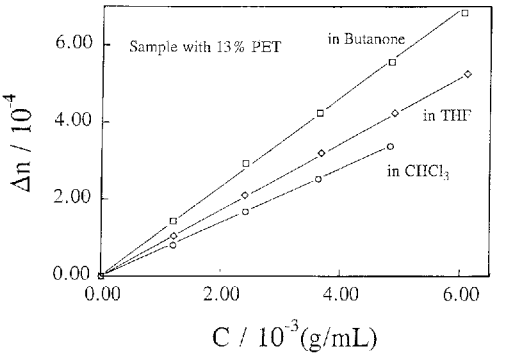

Fig. 9. Possible arrangement of the novel differential refractometer with an existing laser light scattering spectrometer

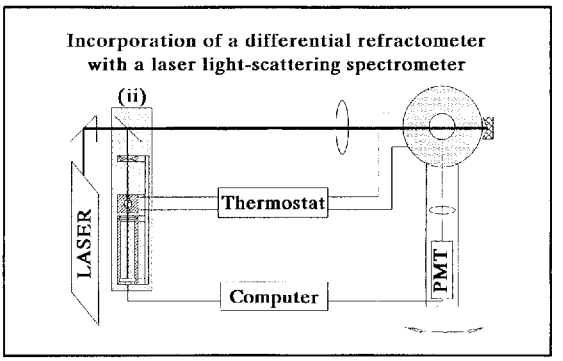

Fig. 10. Concentration dependence of the refractive index difference (Δn) between the polymer solution and solvent for a 13% PET-PCL copolymer. The lines represent the least-square fits to the measured data

placed in the laser light path at 45° reflects laser light by about 4%, and the reflected light is used as the light source. With this design, the light scattering and the refractive index increment can be simultaneously measured under the identical experimental conditions of wavelength and temperature. The details of this novel spectrometer have been described elsewhere [40].

4 Data Analysis

The methods of analyzing data for the concentration and angular dependence of the time-average scattering light intensity and the intensity-intensity time correlation function can be found in many LLS books and related literature. In this section, we will mainly concern ourselves with how to combine static and dynamic LLS results to characterize special polymers in regard not only to the average molar mass, but also to the molar mass and composition distributions.

4.1 Conversion Between Translational Diffusion Coefficient Distribution and Molar Mass Distributions

Though not involving fractionation, DLS allows estimation of the molecular weight distribution of a polymer. The principle is as follows. For a polydisperse polymer consisting of n homologous species, it is well known that $G(D_i)$ for species i at vanishingly small C and q is given by

$$G(D_i) = M_i w_i / \sum_{j=1}^{n} M_j w_j \tag{4.1}$$

where w_i denotes the weight fraction of species i with molecular weight M_i. For a continuous distribution of molecular weight this gives

$$G(D)dD = Mf_w(M)dM / M_w \tag{4.2}$$

where $f_w(M)$ denotes the weight distribution of molecular weight M. Thus, we get

$$f_w(M) = (M_w / M)G(D)(dD / dM) \tag{4.3}$$

Empirically we have for a series of homologous polymers [41]

$$D = k_D M^{-\alpha_D} \tag{4.4}$$

where k_D and α_D are constants. Experimentally, for a flexible polymer, $0.5<\alpha_D<0.6$ in a good solvent and $\alpha_D=0.5$ in a Flory Θ solvent; for a rigid rod-

like chain, $\alpha_D=1$; and for a semi-rigid worm-like chain, $0.6<\alpha_D<1$. With Eq. (4.4), Eq. (4.3) is transformed to

$$f_w(M) = k_D M_w M^{-\alpha_D - 2} G(D) \tag{4.5}$$

which indicates that $f_w(M)$ can be determined if G(D) is obtained by Laplace inversion of Eq. (2.6) and the values of the parameters k_D and α_D are available from separate sources. This is the basic idea of the method which allows information about $f_w(M)$ to be derived by DLS.

Since, as noted above, the success in determining G(D) is actually not in the choice of a computer program for Laplace inversion but reducing the noise level in measured $g^{(1)}(t,q)$. Thus, it is crucial that the solution is cleaned (i.e. "dust-freed") very thoroughly before it is subjected to laser light scattering measurements. For example, in studies conducted by the author, efforts were made to ensure that the relative difference between the measured and calculated baselines did not exceed 0.1%. The error analysis related to the above problem can be found elsewhere [42, 43].

4.2
Scaling of Translational Diffusion Coefficient D with Molar Mass M

4.2.1
Using a Set of Narrowly Distributed Standards

The most straightforward method for calibrating the relationship between D and M is to measure both D and M for a set of monodisperse samples with different molecular weights. In reality, the monodisperse samples have to be replaced by narrowly distributed standards made available either by relevant living polymerization or by fractionation of a broadly distributed sample. However, only a few kinds of polymers, e.g. polystyrene and poly(methyl methylacrylate), can actually be prepared so as to have a sufficiently narrow molecular weight distribution ($M_w/M_n \sim 1.1$), and the fractionation is very time consuming. Thus, the straightforward calibration of the D vs M relation is not always practical.

Figure 11 shows the plot of log(D) versus log (M) for a set of narrowly distributed polystyrene standards in toluene at 20 °C [44]. The line represents a least-square fitting to the data points, giving $D(cm/s)=3.64\times10^{-4}M^{-0.577}$. Using this relation, we were able to estimate the molar mass distribution of polystyrene by using only DLS [45]. However, as noted above, in reality, only a few kinds of polymers can be prepared to have narrow enough distributions of molecular weight. Hence, we often have to satisfy ourselves with more broadly distributed samples having different average molecular weights. This means that special analytical methods have to be developed to calibrate or scale the translational diffusion coefficient D and molar mass M by using from broadly distributed samples. Ideas on this theme are described in the following sections.

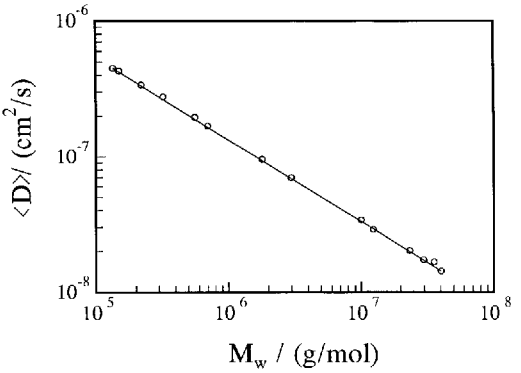

Fig. 11. Double logarithmic plot D vs M for polystyrene in toluene at 20 °C. The line represents a least-square fits to the data points, giving $D(cm/s) = 3.64 \times 10^{-4} M^{-0.577}$ (Ref. 42)

4.2.2
Using Two or More Broadly Distributed Samples

As can be easily shown, it follows from Eqs.(4.4) and (4.5) that

$$M_w = (k_D)^{1/\alpha_D} / \int_0^\infty G(D) D^{1/\alpha_D} dD \tag{4.6}$$

The quantity on the right-hand side is denoted by $M_{w,calc}^{DLS}$. i.e.

$$M_{w,calc}^{DLS} = (k_D)^{1/\alpha_D} / \int_0^\infty G(D) D^{1/\alpha_D} dD \tag{4.7}$$

For any given set of k_D and α_D, it can be calculated when G(D) is determined from DLS measurements. We denote it for a polydisperse sample i by $(M_{w,calc}^{DLS})_i$. Then we get

$$\frac{(M_{w,calc}^{DLS})_i}{(M_{w,calc}^{DLS})j} = \left[\int_0^\infty G_j(D) D^{1/\alpha_D} dD\right] / \left[\int_0^\infty G_i(D) D^{1/\alpha_D} dD\right] \tag{4.8}$$

where $G(D)_i$ is for sample i. The right-hand side can be calculated from measured $G(D)_i$ and $G(D)_j$ for any α_D, and if the chosen value of α_D happens to be equal to that for the system under study, the resulting value of $(M_{w,\,calcd}^{DLS})_i / (M_{w,\,calcd}^{DLS})_j$ should agree with the value of $(M_w)_i / (M_w)_j$ which can be determined by SLS. In reality, the desired α_D will be reached by using a computer program which seeks a minimum of ERROR(α_D) defined by

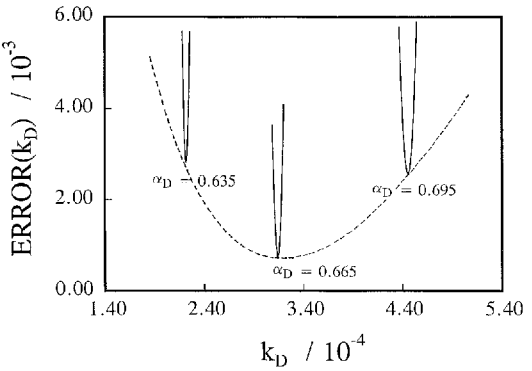

Fig. 12. Plot of ERROR(k_D) calculated with data for five Chitosan samples with different weight average molecular weights. Here the minimum of the dashed curve corresponds to $\alpha_D = 0.665 \pm 0.015$ and $k_D = (3.14 \pm 0.20) \times 10^{-4}$

$$\mathrm{ERROR}(\alpha_D) = \sum_i^N \sum_j^N \left[\frac{(M_w)_i}{(M_w)_j} - \frac{(M_{w,calc}^{DLS})_i}{(M_{w,calc}^{DLS})_j}\right]^2 \tag{4.9}$$

where N is the total number of the polydisperse samples examined.

Next, with the α_D value so determined, we compute $(M_{w,calcd}^{DLS})_i$ for each of the N samples from Eq. (4.7) by varying k_D and seek a k_D value which minimizes ERROR(k_D) defined by

$$\mathrm{ERROR}(k_D) = \sum_i^N \left[\frac{(M_w)_i}{(M_{w,calc}^{DLS})_i} - 1\right]^2 \tag{4.10}$$

Figure 12 depicts a plot of ERROR(k_D) at three values of α_D calculated from SLS and DLS data for five chitosan samples with different M_w. It is seen that for each chosen α_D ERROR(k_D) shows a sharp minimum, but the location and height of the minimum varies significantly with α_D and the minimum becomes the smallest at α_D=0.665 and k_D=3.14×10^{-4}. With these values, the molecular weight distributions of chitosan samples have been successfully characterized [18].

4.3 Combination of LLS with Other Off-line Methods

4.3.1 *Intrinsic Viscosity*

If only one broadly distributed sample is available, we have to resort to another method to determine the relation between D and M. One of them is to estimate α_D from the Mark-Houwink equation for intrinsic viscosity. It is known that the intrinsic viscosity [η] can be scaled with M by the Mark-Houwink equation, i.e.

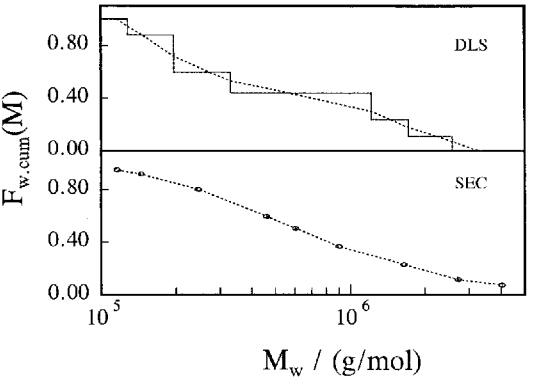

Fig. 13. Comparison of cumulative weight distributions $F_{w,cum}(M)$ $[=\int_M^\infty f_w(M)\,dM]$ obtained by DLS and SEC (size exclusion chromatography) for a linear polyethylene in 1,2,4-trichlorobenzene at 135 °C

$[\eta]=k_\eta M^{\alpha_\eta}$, and according to Flory and also to de Gennes [41, 46], α_D may be equal to $=(\alpha_\eta+1)/3$. With α_D estimated from α_η by this relation, M_w from static LLS and G(D) from dynamic LLS can be used to determine k_D as described above. Chu *et al.* [47,48] successfully applied this method to linear polyethylene in 1,2,4-trichlorobenzene at 135 °C for which α_D was estimated from the reported value of $\alpha_\eta=0.72$. [49]

Figure 13 shows the resulting cumulative weight distribution $F_{w,cum}(M)$ $[=\int_M^\infty f_w(M)\,dM]$ and compares it with the result obtained by high-temperature size exclusion chromatography (SEC). The agreement is reasonably good, but it should be noted that the weight distribution from LLS is usually narrower and more skewed toward the high molar mass than that from GPC because the scattered light intensity is proportional to the square of molar mass so that higher molar mass species weigh more in LLS.

4.3.2
Gel Permeation Chromatography

The static laser light scattering apparatus used as an on-line GPC detector has been popular for a while. Here, we illustrate another but less known method of combining the results from (gel permeation chromatography) and DLS. The basic principle is as follows: There is a similarity between these two tools in that the translational diffusion coefficient D obtained by DLS and the elution volume V in GPC are related to the hydrodynamic size of a given macromolecule. In a first approximation, if the hydrodynamic size is proportional to the molar mass, we have

$$V = A + B\log(M) \tag{4.11}$$

where A and B are constants similar to k_D and α_D. It should be noted that this approximation simplifies but does not affect the following discussion. Combining of Eqs. (4.4) and (4.11) leads to

$$V = A + B \log(D) \tag{4.12}$$

where $A = A + B \log(k_D)/\alpha_D$ and $B = -B/\alpha_D$. Furthermore, we get from Eq. (4.12)

$$V^2 = A^2 + 2AB \log(D) + B^2 \log^2(D) \tag{4.13}$$

Averaging both sides of Eqs. (4.12) and (4.13) over the concentration profile C(V) in GPC, we obtain

$$\langle V \rangle = A + B \langle \log(D) \rangle \tag{4.14}$$

and

$$\langle V^2 \rangle = A^2 + 2AB \langle \log(D) \rangle + B^2 \langle \log^2(D) \rangle \tag{4.15}$$

where

$$\langle V \rangle = \int_0^\infty VC(V)\ dV$$

and

$$\langle V^2 \rangle = \int_0^\infty V^2 C(V)\ dV \tag{4.16}$$

while

$$\langle \log(D) \rangle = \frac{\int_0^\infty \log(D)C(V)\ dV}{\int_0^\infty C(V)\ dV}$$

and

$$\langle \log^2(D) \rangle = \frac{\int_0^\infty \log^2(D)C(V)\ dV}{\int_0^\infty C(V)\ dV} \tag{4.17}$$

Though not yet theoretically proved, it is usually assumed that the differential area C(V)dV under a GPC curve is proportional to the differential mass of the polymers dW that are contained in the differential elution volume dV. Since dW $\propto f_w(M)dM$, we have

$$C(V)dV \propto f_w(M)dM \tag{4.18}$$

If C(V) is normalized, this gives

$$C(V)dV = f_w(M)dM \tag{4.19}$$

Combining Eqs.(4.3), (4.4) and (4.19), Eq. (4.17) can be rewritten

$$\langle \log(D) \rangle = \frac{\int_0^\infty \log(D)G(D)D^{1/\alpha_D}dV}{\int_0^\infty G(D)D^{1/\alpha_D}dV}$$

and

$$<\log^2(D)> = \frac{\int_0^\infty \log^2(D)G(D)D^{1/\alpha_D}dV}{\int_0^\infty G(D)D^{1/\alpha_D}dV} \tag{4.20}$$

After Eq. (4.19) is multiplied by M, both sides are integrated over the entire range of M to yield

$$M_w = \int_0^\infty MC(V)dV \tag{4.21}$$

Elimination of M from the right-hand side using the relation $D=k_DM^{-\alpha D}$ and Eq. (4.12) transforms Eq. (4.21) to

$$M_w = k_d^{1/\alpha_D} \int_0^\infty 10^{(A-V)/(\alpha_D B)} C(V)\, dV \tag{4.22}$$

which is combined with Eq. (4.6) for M_w to give

$$\left[\int_0^\infty 10^{(A-V)/(\alpha_D B)} C(V)\, dV\right]\left[\int_0^\infty G(D)D^{1/\alpha_D} dD\right] = 1 \tag{4.23}$$

This equation contains only one unknown parameter α_D. For a chosen α_D, we first calculate $<\log(D)>$ and $<\log^2(D)>$ using Eq (4.20), then calculate **A** and **B** by solving Eqs.(4.14) and (4.15) with $<V>$ and $<V^2>$ computed from the GPC diagram, and finally calculate the left side of Eq. (4.23). By iteration, we can find a value of α_D which may minimize the difference between the left and right sides of Eq. (4.23). For the α_D so obtained, we can calculate k_D from either Eq. (4.6) or (4.22) by using M_w determined directly from static LLS and C(V) from SEC or G(D) from dynamic LLS. With **A**, **B**, k_D and α_D, we are ready to calculate *A* and *B*. In this way, we can calibrate not only the M vs V relation, but also the M vs D by a single process on only one broadly distributed sample. This method has been tested and applied in the characterization of gelatin in water [50, 51].

5 Applications

When the relation between D and M is established, we can easily convert G(D) obtained by dynamic LLS into a differential molecular weight distribution, such as $f_w(M)$. We have successfully applied the above methods to various kinds of polymeric and colloidal systems, such as for Kevlar [15, 23], fluoropolymers (Tefzel & Teflon) [12, 30–35, 52], epoxy [53–55], polyethylene [56, 57], water-soluble polymers [18, 50–51, 58, 59], copolymers [60–62], thermoplastics [63–65] and colloids [66–72]. Three of those applications are illustrated below.

5.1
Segmented Copolymers

We consider a copolymer sample consisting of monomers A and B. The sample is generally polydisperse in both molecular weight and chain composition. We suppose that the copolymer species i is characterized by the molecular weight M_i and the composition w_{Ai} which is the weight fraction of A in the chain of that species. It is assumed that no composition heterogeneity exists in the chains of the same length. For homopolymers the refractive index increment (at infinite dilution) does not depend, in a good approximation, on the molecular weight of the chain, but is equal to that of the entire sample. For copolymers this is not the case, and, according to the theory of light scattering, Eq. (4.1) for G_i may be replaced by

$$G_i = (\nu_i / \nu)^2 M_i w_i / \sum_j M_j w_j \tag{5.1}$$

where ν_i is the refractive index increment due to the copolymer species i, ν that of the entire sample, and w_i the weight fraction of the copolymer species i. When the molecular weight distribution may be treated as continuous. Equation (5.1) is generalized to

$$G(D)dD = (\nu(M)/\nu)^2 M f_w(M) M dM \tag{5.2}$$

where, as before, $f_w(M)$ denotes the weight distribution of M, and $\nu(M)$ is the refractive index increment due to the chains of molecular weight M. Note that $\nu(M)$ depends on $w_A(M)$, which is the continuous version of w_{Ai}. We assume that this dependence is represented by

$$\nu(M) = \nu_A w_A(M) + \nu_B[1 - w_A(M)] \tag{5.3}$$

where ν_A and ν_B are the refractive index increments of the homopolymers consisting respectively of A and B.

Corresponding to Eq. (4.3) for homopolymers, we introduce $f_{w,app}(M)$, an apparent weight distribution function of M, by

$$f_{w,app}(M) = (M_w / M) G(D)(dD/dM) \tag{5.4}$$

With Eq. (4.4) (assumed to hold for copolymers too), this gives

$$f_{w,app}(M)/M_w = (1/k_D)^{2/\alpha_D} G(D) D^{1+(2/\alpha_D)} \tag{5.5}$$

Therefore, $f_{w,app}(M)/M_w$ can be calculated from DLS determination of G(D) along with Eq. (4.4) when k_D and α_D are known separately. On the other hand, substituting Eq. (5.2) together with Eq. (5.3) into Eq. (5.4), we get

$$f_{w,app}(M)/M_w = \nu^{-2}[\nu_A w_A(M) + \nu_B(1 - w_A(M))]^2 f_w(M) \quad (5.6)$$

Now, we choose two solvents 1 and 2 for a given copolymer. Since $f_{w,app}(M)$, ν, ν_A, and ν_B vary with solvent, their values in solvent i are denoted by $f_{w,app}(M)^{(i)}$, $\nu^{(i)}$, $\nu_A{}^{(i)}$, and $\nu_B{}^{(i)}$. Then it follows from Eq. (5.6) that

$$\frac{f_{w,app}{}^{(1)}(M)}{f_{w,app}{}^{(2)}(M)} = \left\{\frac{\nu^{(2)}}{\nu^{(1)}}\frac{w_A(M)\nu_A{}^{(1)} + [1 - w_A(M)]\nu_B{}^{(1)}}{w_A(M)\nu_A{}^{(2)} + [1 - w_A(M)]\nu_B{}^{(2)}}\right\}^2 \quad (5.7)$$

The ratio on the left-hand side can be obtained as a function of M since $f_{w,app}(M)^{(i)} / M_w$ can be determined, as described above, from experimental information. Thus, Eq. (5.7) allows determination of $w_A(M)$, the chain composition distribution when all other parameters on its right-and side are measured by differential refractometry. Once $w_A(M)$ is known, we are ready to compute $\nu(M)$ from Eq. (5.3), $f_w(M)$ from Eq. (5.6), and finally M_w [59].

Figure 14 shows PLS determined – G(D)s by Eq. (5.3) for low-mass (○) and high-mass (❑) segmented copolymer poly(ethylene terephthalate-co-caprolactone)s (PET-PCL) containing 13% PET in tetrahydrofuran (THF) at 25 °C. Repeating the measurements on these samples in another solvent chloroform should lead to a new set of G(D)s, which allows Eq. (5.7) to be used to calculate $w_{PET}(M)$.

Figure 15 shows the results from such calculations for low mass (○) and high mass (❑)13% PET-PCL samples. We see that the PET content increases with increasing M for $M < \sim 4\times10^4$ and approaches a constant value of ~14% in the high molar mass range. For the 58% PET-PCL sample, the composition distribution is nearly constant. The composition of the high-molar mass 13% PET-PCL sample overlaps with that of the low mass 13% PET-PCL sample in the same molec-

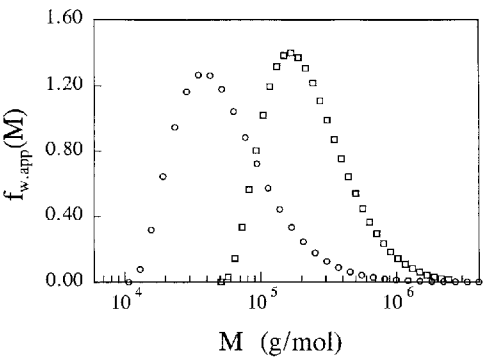

Fig. 14. Apparent weight distributions calculated from the translational diffusion coefficient distributions corresponding to low-mass (○) and high-mass (❑) copolymer segmented poly(ethylene terephthalate-*co*-caprolactone) (PET-PCL) containing 13% PET in tetrahydrofuran (THF) at 25 °C

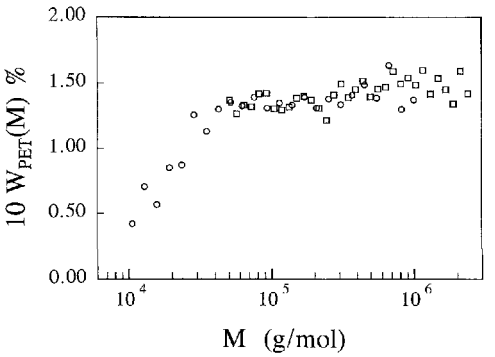

Fig. 15. Estimate of the chain composition distributions for low mass (○) and high mass (❑)13% PET-PCL samples

ular weight range. This indirectly indicates that the estimation of the composition distribution is reasonable. The lower content of PET in the low molar mass range can be attributed to the two-step synthesis [59–62].

5.2
A Polymer Mixture Containing Individual Chains and Clusters

If a mixture is made of individual polymer chains and polymer clusters, the measurement of static LLS will lead to an apparent weight-average molar mass $M_{w,app}$ which is expressed by

$$M_{w,app} = M_{w,L}x_L + M_{w,H}x_H \tag{5.8}$$

where the subscripts "L" and "H" denote low molar mass linear polymer chains and high molar mass polymer clusters, respectively, and x_L and x_H are their weight fractions with $x_L+x_H=1$. If the linear chains and clusters are significantly different in the hydrodynamic size, dynamic LLS will detect two distinct peaks in the measured G(D), with one peak corresponding to the linear chains and the other to clusters.

Figure 16 shows G(D) of a simulated polymer mixture at two scattering angles ("○", 14° and "❑", 17°). The mixture consists of two polystyrene standards having distinctly different weight average molar masses (3.0×10^5 and 5.9×10^6 g/mol) and a high mass polystyrene which is used to simulate the polymer cluster [66]. The area ratio A_r of the two peaks is expressed by

$$A_r = \frac{A_L}{A_H} = \frac{\int_0^{\gamma} G_L(D)\ dD}{\int_{\gamma}^{\infty} G_H(D)\ dD} = \frac{M_{w,L}x_L}{M_{w,H}x_H} \tag{5.9}$$

with γ the cutoff translational diffusion coefficient between $G_L(D)$ and $G_H(D)$. In practice, the values of A_r at finite scattering angles must be extrapolated to

$q \rightarrow 0$. Figure 17 shows this extrapolation of the A_r for the two peaks in Fig. 16. With Eqs. (5.8) and (5.9), $M_{w,app}$ from static LLS and A_r from dynamic LLS allow $M_{w,L}x_L$ and $M_{w,H}x_H$ to be computed. In principle, by knowing any one of the four parameters ($M_{w,L}$, $M_{w,H}$, x_L and x_H), we should be able to determine the remaining three parameters. This method has been thoroughly tested with mixtures of polystyrene standards [64]. As for a particular polymer mixture, we should find a way allowing determination of one of the four parameters. For example, in the study of polymer association, we can determine the $M_{w,L}$ of starting individual polymer chains, and in the study of the gelation process, we can use a filtration method to remove large microgels, so that the weight fractions of x_L and x_H can be subsequently determined. This method has been used to characterize novel thermoplastic polymers with phenolphthalein in their backbone chains [61–63].

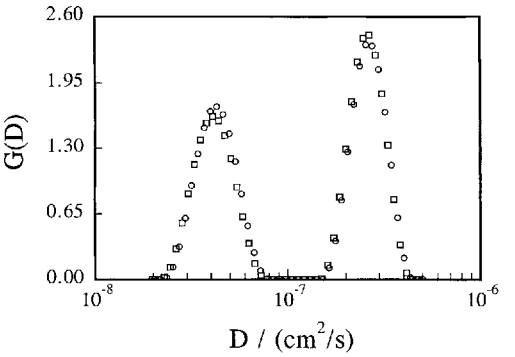

Fig. 16. Translational diffusion coefficient distributions G(D) of a simulated polymer mixture at two scattering angles ("❑", 17° and "○", 14°). The mixture contains two polystyrene standards of distinctly different weight average molar masses (3.0×10^5 and 5.9×10^6 g/mol) and a high mass polystyrene

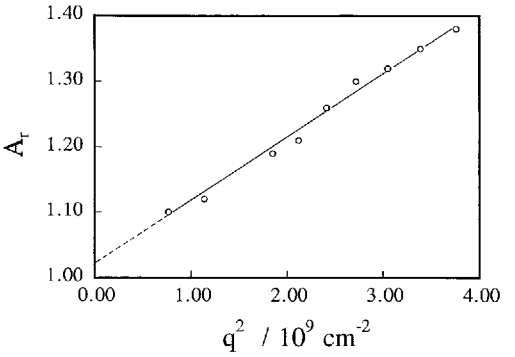

Fig. 17. q^2-dependence of the area ratio ($A_r = A_L / A_H$) for the two peaks of the translational diffusion coefficient distribution shown in Fig. 16

5.3 Polymer Colloids

Combination of static and dynamic laser light scattering is also useful to determine not only the size distribution but also the particle structure of polymer colloids such as the adsorbed surfactant layer thickness [73] and the formation of nanoparticles [74, 75]. A recently developed method of determining the density of polymer particles is outlined below to illustrate the usefulness of laser light scattering as a powerful analytical tool for investigating more sophisticated colloidal problems [76–78].

For a colloidal particle of uniform density its molar mass M is proportional to the cube of its radius R, i.e.

$$M=(4/3)\pi R^3 \rho N_A \tag{5.10}$$

where ρ is the particle density and N_A the Avogadro constant. The diffusion coefficient D of the particle (at infinite dilution) is related to the Stokes radius R_h by

$$D = (k_B T / 6\pi\eta)(1 / R_h) \tag{5.11}$$

where k_B is the Boltzmann constant, T the absolute temperature, and η the solvent viscosity. We assume that R_h is larger than R by the thickness b of the solvated layer, i.e.

$$R_h = R + b \tag{5.12}$$

Substituting this into Eq. (5.11) and using Eq. (5.10) for R, we obtain

$$D = F(k_B T/6\pi\eta)\,(4\pi\rho N_A)^{1/3}\, M^{-1/3} \tag{5.13}$$

with

$$F = 1/[1+b(4\pi\rho N_A/M)^{1/3}] \tag{5.14}$$

Comparing Eq. (5.13) with the relation $D=k_D M^{-\alpha D}$ and considering $b<<R$, we find approximately

$$\alpha = 1/3 \tag{5.15}$$

$$k_D = F(k_B T/6\pi\eta)(4\pi\rho N_A)^{1/3} \tag{5.16}$$

Thus, with M in Eq. (5.14) replaced by M_w, it follows from Eq. (4.6) that

$$M_w = \frac{1}{[1+b(4\pi\rho N_A/M_w)^{1/3}]^3}\left(\frac{4\pi\rho N_A}{3}\right)\left(\frac{k_B T}{6\pi\eta}\right)^3 \Big/ \int_0^\infty G(D)D^3 dD \tag{5.17}$$

This equation contains two unknown parameters (b and ρ), and if we know one of them, the other can be calculated from M_W and G(D). With this idea, it was found that the average density of the polystyrene microspheres made of a few uncrosslinked chains is slightly lower than that of bulk polystyrene or conventional polystyrene latex.

6 Conclusions

This review has shown that static and dynamic laser light scattering (LLS) combined provide a very powerful method for polymer characterization. LLS has advantages over other polymer characterization methods, which include ultracentrifugation and chromatography, in such features as speed, non-perturbation and extreme dissolution conditions (high temperature or strong acid). The most important advantage is that the calibration is independent of the particular LLS instrument used. However, the LLS method for the determination of mass distributions described in this paper is disadvantageous in that its resolution is not as high as the fractionation methods, especially for samples whose mass distributions have closely packed peaks. The LLS method should play a definite role in circumstances where polymers intractable by conventional characterization methods have to be treated. In principle, dynamic LLS can be used together with other polymer characterization methods which take advantage of the dependence of the hydrodynamic volume on molecular weight.

Acknowledgments. My special thanks to Professor Benjamin Chu who led me to the laser light scattering field fourteen years ago. I am also indebted to my former colleagues at Stony Brook (USA) and in BASF (Germany) for their cooperation, to my collaborators in China for their help, and to my postgraduate students for their dedication to our research projects in the past years. The financial support of the Research Grants Council of Hong Kong Government from 1993 to 1996 is gratefully acknowledged. I would also like to thank Professor Hiroshi Fujita for his constant guidance and encouragement in the process of writing this review.

References and Notes

1. Flory PJ, Krigbaum WR (1950) J Chem Phys 18:1086
2. Grimley TB (1952) Proc Roy Soc (London) A212:339
3. Chien JY, Shih LH, Yu SC (1958) J Polym Sci 26(119):117
4. Huglin MB (1972) Light scattering from polymer solution. Academic, London
5. Chu B, Fytas G (1982) Macromolecules 15:562
6. Ford NC (1983) In: Dahneke B (ed) Measurement of suspended particles by quasi-elastic light scattering. Wiley, New York
7. Pecora R (ed) (1985) Dynamic light scattering. Plenum, New York
8. Brown W (ed) (1996) Light scattering: principles and development. Clarendon, Oxford
9. Chu B (1991) Laser light scattering. Academic. New York, 2nd edn
10. Berne BJ, Pecora R (1976) Dynamic light scattering. Plenum, New York
11. Zimm BH (1948) J Chem Phys 16:1099
12. Chu B, Wu C (1987) Macromolecules 20:2642
13. Russo PS (1993) In: Brown W (ed) Dynamic light scattering, Chap 12. Oxford University Press, New York

14. Chu B, Ying Q, Wu C, Ford J (1984) Polymer Communications 25:211
15. Chu B, Ying Q, Wu C (1985) Polymer 26:1408
16. Ying Q, Chu B (1984) Die Makromolekulare Chemie, Rapid Communication 5:785
17. Stockmayer WH, Schmidt M (1984) Macromolecules 17:509
18. Wu C, Zhou SQ, Wang W (1995) Biopolymer 35:385
19. Koppel DE (1972) J Chem Phys 57:4814
20. Livesey AK, Licinio P, Delaye M (1986) J Chem Phys 84:5102
21. McWhirter JG, Pike ER (1978) J Phys A 11:1729
22. Chu B, Ford JR, Dhadwal HS (1983) Methods Enzymol 117:256
23. Chu B, Wu C, Ford JR (1985) J Colloid Interface Sci 105:473
24. Provencher SW (1976) J Chem Phys 64:2772
25. Chu B, Wu C, Ford JR (1985) J Colloid Interface Sci 105:473
26. Bushuk W, Benoit H (1958) Can J Chem 36:1616
27. Chu B, Ying Q, Lee DC, Wu DQ (1985) Macromolecules 18:1962
28. Stockmayer WH, Moore LD, Fixman M, Epstein BN (1955) J Polym Sci 16:517
29. Wu C, Woo KF, Luo XL, Ma DZ (1994) Macromolecules 27:6055
30. Chu B, Wu C (1987) Macromolecules 20:93
31. Wu C, Buck W, Chu B (1987) Macromolecules 20:98
32. Chu B, Wu C, Zuo J (1987) Macromolecules 20:700
33. Chu B, Wu C, Buck W (1988) Macromolecules 21:397
34. Chu B, Wu C, Buck W (1989) Macromolecules 22:831
35. Wu C (1992) Makromol Chem, Makromol Symp 61:377
36. Obasa M, Nakamura H, Takasaka M, Keto T, Nagasawa M (1993) Polym J 25:301
37. Application Notes LS7 Chromatix, Mountain View, California, USA
38. Baltog I, Ghita C, Ghita L (1970) Eur Polym J 6:1299
39. Application Notes Optilab 903, Wyatt Technology, Santa Barbara, California, USA
40. Wu C, Xia KQ (1994) Review of Scientific Instruments 65:587
41. de Gennes PG (1979) Scaling concepts in polymer physics. Cornell University Press, Ithaca, NY
42. Raczek J (1983) Eur Polym J 19:607
43. Nordmeier E, Lechner MD (1989) Polym J 21:623
44. Appelt B, Meyerhoff G (1980) Macromolecules 13:657
45. Wu C, Zhang YB, Yan XH, Cheng RS (1995) Acta Polymerica Sinica 3:349
46. Flory PJ (1953) Principles of polymer chemistry. Cornell University Press, Ithaca, NY
47. Chu B, Onclin M, Ford JR (1984) J Phys Chem 88:6566
48. Pope J, Chu B (1984) Macromolecules 17:2633
49. Cervenka A (1973) Makromol Chem 170:239
50. Wu C (1993) Macromolecules 26:5423
51. Wu C (1994) J Polym Sci Polym Phys Ed 32:803
52. Wu C, Chu B (1986) Macromolecules 19:1285
53. Wu C, Zuo J, Chu B (1989) Macromolecules 22:633
54. Wu C, Zuo J, Chu B (1989) Macromolecules 22:838
55. Wu C, Chu B, Stell G (1992) Makromol Chem, Makromol Symp 45:75
56. Wu C, Lilge D (1993) J Appl Polym Sci 50:1753
57. Wu C (1993) J Appl Polym Sci 54:969
58. Zhou SQ, Fan SF, Au-yeung SCF, Wu C (1995) Polymer 36:1341
59. Wu C, Wu PQ, Ma XQ (1995) J Polym Sci Polym Phys Ed, in press
60. Wu C, Ma D, Luo X, Chan KK, Woo KF (1994) J Appl Polym Sci 53:1323
61. Wu C, Woo KF, Luo X, Ma D (1994) Macromolecules 27:6055
62. Woo KF, Wu C (1995) J Appl Polym Sci 57:1285
63. Bo S, Siddiq M, Wu C (1996) Macromolecules 29:2989
64. Wu C, Siddiq M, Bo B (1995) Macromolecules 29:3157
65. Siddiq M, Li BY, Wu C (1996) J Appl Polym Sci 60: 1995
66. Wu C, Siddiq M, Woo KF (1995) Macromolecules 28:4914
67. Wu C (1994) Macromolecules 27:298

68. Wu C (1994) Macromolecules 27:7099
69. Wu C, Qian RY, Napper DH (1995) Macromolecules 28:1592
70. Zhou SQ, Wu C (1995) Macromolecules 28:5225
71. Wu C (1994) Chinese J Polym Sci 12:323
72. Wu C, Chan KK (1995) J Polym Sci Polym Phys Ed 33:919
73. Wu C (1994) Macromolecules 27:298, 7099
74. Li M, Jiang M, Wu C (1997) Macromolecules 30:2201
75. Wu C, Chen M, Akashi M (1997) Macromolecules 30:2187
76. Wu C, Chan KK (1994) J Polym Sci, Polym Phys Ed 33:919
77. Wu C, Qian RY, Napper DH (1994) Macromolecules 28:1592
78. Gao J, Zhou SQ, Wu C (1996) Polym Engineering Sci 36:2968

Editor: Prof. Hiroshi Fujita
Received: September 1997